A Strongly Coupled Mixed Valence State Between Ru_3 Clusters. Intramolecular Electron Transfer on the Infrared Vibrational Time Scale in a Pyrazine (pz) Bridged Dimer of Triruthenium Clusters, $[\{Ru_3(\mu_3\text{-}O)(\mu\text{-}CH_3CO_2)_6(CO)(abco)\}_2(\mu\text{-}pz)]$ (abco = 1-azabicyclo[2,2,2]octane)

Tadashi Yamaguchi, Naoyuki Imai, Tasuku Ito,* and Clifford P. Kubiak†

Department of Chemistry, Graduate School of Science, Tohoku University, Sendai 980-8578

†Department of Chemistry and Biochemistry, University of California, San Diego, La Jolla, CA 92093-0358, USA

(Received December 20, 1999)

A pyrazine bridged dimer of triruthenium clusters $[\{Ru^{III}_2Ru^{II}(\mu_3\text{-}O)(\mu\text{-}CH_3CO_2)_6(CO)(abco)\}_2(\mu\text{-}pz)]$ (abco = 1-azabicyclo[2,2,2]octane, pz = pyrazine) gives an inter-cluster mixed valence state upon one electron reduction. The splitting of the reduction waves in cyclic voltammetry, ΔE, was 470 mV. This corresponds to a comproportionation constant for formation of the mixed valence state of 9.0×10^7. The IR spectrum of the mixed valence species in the ν(CO) region, measured by reflectance IR spectroelectrochemistry, showed a completely coalesced ν(CO) band. This represents delocalized redox behavior on the infrared vibrational timescale. The rate constant for intramolecular electron transfer was estimated to be 1×10^{12} s^{-1} at -18 °C by simulating the ν(CO) absorption bandshape. The mixed valence complex showed an intervalence charge transfer (ICT) band at 12500 cm^{-1}. Hush analysis provides a spectroscopic estimate of H_{AB} to be 2490 cm^{-1}. Crystal structures of $[\{Ru^{III}_2Ru^{II}(\mu_3\text{-}O)(\mu\text{-}CH_3CO_2)_6(CO)(abco)\}_2(\mu\text{-}pz)]\cdot2CH_2Cl_2$ and its precursor, $[Ru^{III}_2Ru^{II}(\mu_3\text{-}O)(CH_3CO_2)_6(CO)(abco)_2]\cdot CH_2Cl_2$, were determined by X-ray crystallography. Trends in Ru–O(oxo) and Ru–O(acetate) distances in these compounds show that the divalent site is localized on the Ru center attached to the carbonyl ligand.

In the Robin–Day classification scheme,[1] a class II mixed valence state between two interacting redox centers is characterized by a double-well ground state potential energy surface with a defined thermal barrier to electron transfer. The estimation of intramolecular electron transfer rate constants in class II systems can be made directly by a variety of experimental techniques including Mössbauer spectroscopy,[2] or indirectly by Hush analysis of the intervalence charge transfer band.[3] More recently, Cannon estimated a rate constant on the order of 10^{11} s^{-1} for electron transfer in a trinuclear mixed valence iron(III,III,II) complex based on IR spectroscopic analysis.[4] Masuda et al. evaluated a rate constant on the order of 10^{12} s^{-1} for intramolecular electron transfer within the mixed valence monocationic state of a biferrocene based on ^{1}H NMR T_1 measurements.[5] Here, we describe our ongoing studies of a series of pyrazine (pz) and 4,4′-bipyridine (4,4′-bpy) bridged dimers of trinuclear ruthenium complexes, $[\{Ru^{III}_2Ru^{II}(\mu_3\text{-}O)(\mu\text{-}CH_3CO_2)_6(CO)(L)\}_2(\mu\text{-}BL)]^-$ (Chart 1). Many of these complexes afford stable inter-cluster mixed valence complexes upon one-electron reduction. In the mixed valence states, a clear relationship between inter-cluster electronic interaction (H_{AB}) and infrared ν(CO) bandshape has been identified.[6,7] In the most rapidly exchanging systems, electron transfer rate constants estimated by NMR-like Bloch equation analysis are on the order of 10^{11} s^{-1}. The measured intramolecular electron transfer rate constants depend strongly on the nature of not only the bridging ligand (BL), but also the

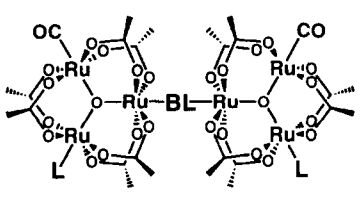

L \ BL	pz	4,4'-bpy
abco	This work	—
dmap	ref. 6,7	ref.7
py	ref. 6,7	ref.7
cpy	ref. 6,7	ref.7

BL = 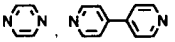 (pz) (4,4'-bpy)

L = 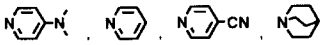 (dmap) (py) (cpy) (abco)

Chart 1.

terminal ligand (L). In the systems where intramolecular rate constants could be estimated by Marcus–Hush analysis, the rate constants determined from IR spectra were found to be faster by nearly two orders of magnitude.[6,7] In as much as the relationships between IR spectroscopic line shape, electron transfer dynamics, and electron transfer theory need to be refined, further work is required. In the present paper, we show that selection of the strongest donor ligand yet investigated by us, L = abco (1-azabicyclo[2,2,2]octane) leads to a dimer of ruthenium trimers [{$Ru^{III}_2Ru^{II}(\mu_3$-O)(μ-$CH_3CO_2)_6$(CO)-(abco)}$_2(\mu$-pz)] (**1**) with an inter-cluster mixed valence state that shows the fastest rate of intramolecular electron transfer ever observed by infrared methods.

Results and Discussion

Synthesis of [{$Ru^{III}_2Ru^{II}(\mu_3$- O)$(CH_3CO_2)_6$(CO)-(abco)}$_2(\mu$-pz)] (1). Complex **1** was synthesized according to Eq. 1 and isolated in good yield.

$$2[Ru^{III}_2Ru^{II}(\mu_3\text{-O})(CH_3CO_2)_6(CO)(abco)_2] + pz \longrightarrow [\{Ru^{III}_2Ru^{II}(\mu_3\text{-O})(CH_3CO_2)_6(CO)(abco)\}_2(\mu\text{-pz})] + 2\ abco. \quad (1)$$

This synthetic method differs from those employed for the preparation of the analogous Ru_3 dimers with pyridyl ligands at the terminal (L) positions (Chart 1). The compounds with terminal pyridyl ligands were prepared by the synthetic strategy which we refer to as the "metal complex as metal" and "metal complex as ligand" approach[8,9] (Eq. 2).

$$[Ru^{III}_2Ru^{II}(\mu_3\text{-O})(CH_3CO_2)_6(CO)(L)(H_2O)] + [Ru^{III}_2Ru^{II}(\mu_3\text{-O})(CH_3CO_2)_6(CO)(L)(BL)] \longrightarrow [\{Ru^{III}_2Ru^{II}(\mu_3\text{-O})(CH_3CO_2)_6(CO)(L)\}_2(\mu\text{-BL})]. \quad (2)$$

The mixed abco/aqua complex, [$Ru_3(\mu_3$-O)$(CH_3CO_2)_6$(CO)-(abco)(H_2O)] ("metal complex as metal") could not be isolated. In general, for pyridyl ligand complexes the reaction analogous to Eq. 1 does not proceed. Thus, it is somewhat surprising that the reaction of Eq. 1 went smoothly to completion. This can be explained on the basis of steric constraints to the coordinating ability of the abco ligand to this type of Ru_3 cluster, in spite of the ligand's high pK_a value (11.15) (vide infra).

Structure of [{$Ru_3(\mu_3$-O)$(CH_3CO_2)_6$(CO)(abco)}$_2(\mu$-pz)]·2CH_2Cl_2(1·2CH_2Cl_2). The structure of **1**·2CH_2Cl_2 has been determined by X-ray analysis. Crystallographic and structural data are listed in Table 1. Selected interatomic distances and bond angles are collected in Table 2. Figure 1 shows an ORTEP drawing of **1**. The compound is, as designed, a pyrazine-bridged Ru_3 dimer with CO and abco ligands on each Ru_3 unit. This is the first report of the X-ray structure of a dimer of triruthenium clusters based on {$Ru_3(\mu_3$-O)$(CH_3CO_2)_6$} cores. There is a crystallographic inversion center located at the center of the bridging pyrazine. The Ru_3 triangle of each cluster is decidedly isosce-

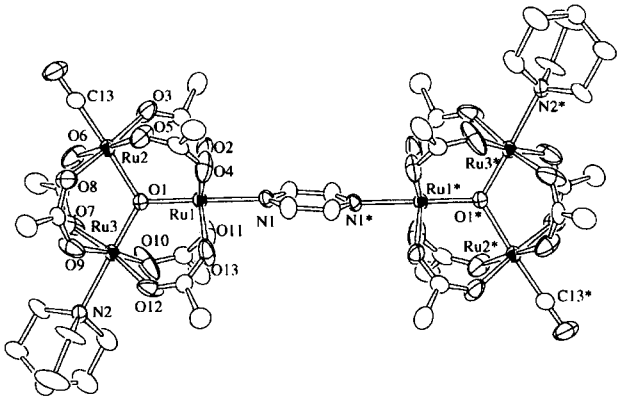

Fig. 1. ORTEP drawing of [{Ru_3(O)$(CH_3COO)_6$(CO)-(abco)}$_2(\mu$-pz)] (**1**) in **1**·2CH_2Cl_2. Ellipsoids are drawn at the 50% probability level. For clarity, hydrogen atoms are omitted and only one of the two disordered abco ligand is depicted.

Table 1. Crystallographic Data for [{$Ru_3(\mu_3$-O)$(CH_3COO)_6$(CO)(abco)}$_2(\mu$-pz)]·2CH_2Cl_2 (**1**·2CH_2Cl_2) and [$Ru_3(\mu_3$-O)$(CH_3CO_2)_6$(CO)$(abco)_2$]·CH_2Cl_2 (**2**·CH_2Cl_2)

	1·2CH_2Cl_2	**2**·CH_2Cl_2
Empirical formula	$Ru_6O_{28}C_{46}N_4H_{70}Cl_4$	$Ru_3O_{14}C_{28}N_2H_{46}Cl_2$
Formula weight	1875.30	1008.79
Crystal system	Triclinic	Orthorhombic
Space group	$P\bar{1}$ (#2)	$Pna2_1$ (#33)
a/Å	12.1044(9)	19.546(1)
b/Å	12.489(1)	16.376(1)
c/Å	13.559(1)	12.1578(9)
V/Å^3	1700.6(2)	3891.6(4)
Z	1	4
D_{calc}/g cm^{-3}	1.831	1.722
μ(Mo $K\alpha$)/cm^{-1}	15.36	13.49
Radiation	Mo $K\alpha$ (λ = 0.71073 Å)	Mo $K\alpha$ (λ = 0.71073 Å)
Temperature/K	203.15	R.T.
$2\theta_{max}$/deg	50.0	55.2
Residuals: $R1$;[a] $wR2$[b]	0.041; 0.126	0.038; 0.130

a) $R1 = \sum||F_o| - |F_c||/\sum|F_o|$. b) $wR2 = [\sum w(|F_o|^2 - |F_c|^2)^2/\sum w|F_o|^4]^{1/2}$, $w = [\sigma^2(F_o^2)+(0.1\times(F_o^2+2F_c^2)/3)^2]^{-1}$.

Table 2. Selected Interatomic Distances (Å) and Angles (deg) for $[\{Ru_3(O)(CH_3COO)_6(CO)(abco)\}_2(\mu\text{-}pz)]\cdot 2CH_2Cl_2$ ($\mathbf{1}\cdot 2CH_2Cl_2$) and $[Ru_3(\mu_3\text{-}O)(CH_3CO_2)_6(CO)(abco)_2]\cdot CH_2Cl_2$ ($\mathbf{2}\cdot CH_2Cl_2$)

	$\mathbf{1}\cdot 2CH_2Cl_2$	$\mathbf{2}\cdot CH_2Cl_2$		$\mathbf{1}\cdot 2CH_2Cl_2$	$\mathbf{2}\cdot CH_2Cl_2$		$\mathbf{1}\cdot 2CH_2Cl_2$	$\mathbf{2}\cdot CH_2Cl_2$
				Distances (Å)				
Ru1–O1	1.889(5)	1.894(3)	Ru1–O2	2.037(4)	2.07(2)	Ru1–O4	2.041(5)	2.01(1)
Ru1–O11	2.041(5)	2.02(1)	Ru1–O13	2.034(5)	2.04(1)	Ru1–N1	2.115(7)	2.261(4)
Ru2–O1	2.057(4)	2.065(3)	Ru2–O3	2.063(5)	2.09(1)	Ru2–O5	2.068(5)	2.04(1)
Ru2–O6	2.064(5)	2.07(1)	Ru2–O8	2.070(5)	2.06(1)	Ru2–C13	1.838(8)	1.851(6)
Ru3–O1	1.896(3)	1.888(3)	Ru3–O7	2.024(6)	2.02(2)	Ru3–O9	2.025(6)	2.04(1)
Ru3–O10	2.023(8)	2.03(1)	Ru3–O12	2.029(6)	2.02(1)	Ru3–N2	2.252(4)	2.272(4)
Ru1···Ru2	3.3973(9)	3.4217(5)	Ru1···Ru3	3.2892(8)	3.2979(5)	Ru2···Ru3	3.4340(5)	3.4084(6)
Ru1···Ru1*	7.011(1)							
				Angles (deg)				
O1–Ru1–O2	95.3(2)	94.5(4)	O1–Ru1–O4	95.1(2)	94.3(4)	O1–Ru1–O11	95.0(2)	91.9(4)
O1–Ru1–O13	94.9(2)	94.7(4)	O2–Ru1–N1	85.1(2)	85.9(4)	O4–Ru1–N1	85.8(3)	86.9(4)
O11–Ru1–N1	84.1(2)	87.8(4)	O13–Ru1–N1	84.6(2)	84.0(4)	O1–Ru1–N1	179.0(2)	178.7(3)
O1–Ru2–O3	93.5(2)	91.5(4)	O1–Ru2–O5	91.4(2)	90.5(4)	O1–Ru2–O6	89.8(2)	90.4(4)
O1–Ru2–O8	91.0(2)	92.9(4)	O3–Ru2–C13	87.3(3)	87.7(5)	O5–Ru2–C13	91.0(3)	87.3(6)
O6–Ru2–C13	87.8(3)	91.8(6)	O8–Ru2–C13	88.3(3)	87.9(5)	O1–Ru2–C13	177.5(3)	177.6(3)
O1–Ru3–O7	94.6(2)	92.3(5)	O1–Ru3–O9	94.0(2)	95.3(4)	O1–Ru3–O10	93.2(2)	95.1(4)
O1–Ru3–O12	94.1(2)	93.0(5)	O7–Ru3–N2	87.9(2)	86.5(5)	O9–Ru3–N2	85.5(2)	84.6(5)
O10–Ru3–N2	87.4(2)	86.1(4)	O12–Ru3–N2	83.4(2)	87.1(5)	O1–Ru3–N2	177.4(2)	178.8(4)
Ru1–O1–Ru2	118.8(2)	119.5(2)	Ru1–O1–Ru3	120.7(2)	121.4(2)	Ru2–O1–Ru3	120.5(3)	119.1(2)

les. The Ru1···Ru2 and Ru2···Ru3 distances (3.3973(9) and 3.4340(5) Å) are significantly longer than the Ru1···Ru3 distances (3.2892(8) Å). This arises from coordination of the strongly π acidic CO ligand to Ru2. The strong trans influence of the CO ligand results in the lengthening of the Ru2–O1 bond (2.057(4) Å) as compared to the Ru1–O1 and Ru3–O1 bonds (1.889(5) and 1.896(3) Å). The isosceles triangle found in **1** is similar to that reported in $[Ru_3(\mu_3\text{-}O)(CH_3CO_2)_6(CO)(mbpy^+)_2](ClO_4)_2\cdot 2DMF$ ($mbpy^+$ = methylbipyridiniumion) in which Ru–(μ_3-O) distances at the CO and $mbpy^+$ sites are 2.039(11) and 1.894(6) Å, respectively.[10] The isosceles triangular Ru_3 geometries in these compounds can be understood to result from valence-trapping. The CO ligand stabilizes Ru^{II}, a normal consequence for strong π acceptors. Thus, Ru2 bound to the CO ligand in **1** is formally in the Ru^{II} state, while Ru1 bound to pyrazine and Ru3 bound to abco are in the Ru^{III} state. Additional evidence for the trapped valence description can be found in the Ru–O(acetate) distances. The Ru2–O(acetate) bonds (av. 2.066) at the CO site are significantly longer than the Ru1–O(acetate) bonds (av. 2.039) and the Ru3–O(acetate) bonds (av. 2.025). It is noteworthy that the Ru3–N2(abco) bond (2.252(4) Å) is clearly longer than the corresponding Ru–N(pyridyl ligand) distances found in related Ru_3 complexes with pyridyl ligands (2.126(10)—2.139(3) Å).[10–12] The rather long Ru3–N2 bond (2.252(4) Å) in **1** may be ascribed to the stereochemical consequence of a bulky abco ligand. This result suggests that the coordination ability of the abco ligand is sterically restricted, a view that is consistent with the ease of abco substitution in the synthetic reaction, Eq. 1 (vide supra).

Structure of $[Ru_3(\mu_3\text{-}O)(CH_3CO_2)_6(CO)(abco)_2]\cdot CH_2Cl_2$ ($\mathbf{2}\cdot CH_2Cl_2$). The structure of the Ru_3 monomeric complex, $\mathbf{2}\cdot CH_2Cl_2$, which is a precursor of **1**, was also determined by X-ray analysis. Crystallographic and structural data are listed in Table 1. Selected inter-atomic distances and bond angles are collected in Table 2. Figure 2 shows an ORTEP drawing of **2** in $\mathbf{2}\cdot CH_2Cl_2$. The structural features of the $Ru_3(\mu_3\text{-}O)$ core in **2** are essentially the same as those for **1**. The triangle formed by the three ruthenium ions is isosceles (Ru1···Ru2 = 3.4217(5), Ru1···Ru3 = 3.2979(5), Ru2···Ru3 = 3.4084(6) Å). The trans influence of the CO ligand is apparent in a long Ru2–O(1) distance of 2.065(3) Å. Relatively long Ru–N(abco) distances (Ru1–N1 = 2.261(4), Ru3–N2 = 2.272(4) Å) were also observed. The formal oxidation state of each ruthenium center in **2** is reflected again in Ru–O(acetate) distances (av. 2.028 Å vs. 2.063 Å for Ru2

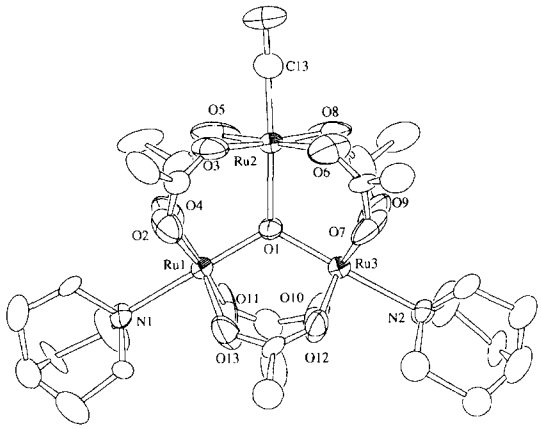

Fig. 2. ORTEP drawing of $[Ru_3(O)(CH_3COO)_6(CO)(abco)_2]$ (**2**) in $\mathbf{2}\cdot CH_2Cl_2$. Ellipsoids are drawn at the 50% probability level. For clarity, only one of the two disordered abco ligand is depicted.

attached to the CO). This is again consistent with Ru2 being in the Ru^{II} state.

Electrochemical Generation of the Inter-Cluster Mixed Valence State. The Ru_3 dimer **1** shows four reversible redox waves in cyclic voltammetry (Fig. 3). Successive two-electron oxidation waves are observed at $E_{1/2}(0/+2) = +0.53$ and $E_{1/2}(+2/+4) = +1.34$ V vs. SSCE. Here, the overall charges of the complexes are expressed in parentheses. Scanning in the cathodic direction, however, shows two single electron reduction waves at -0.84 and -1.31 V vs. SSCE. These processes correspond formally to $Ru^{III}_2Ru^{II}$–pz–$Ru^{III}_2Ru^{II}$/$Ru^{III}_2Ru^{II}$–pz–$Ru^{III}Ru^{II}_2$ $(0/-1)$ and then $Ru^{III}_2Ru^{II}$–pz–$Ru^{III}Ru^{II}_2$/$Ru^{III}Ru^{II}_2$–pz–$Ru^{III}Ru^{II}_2$ $(-1/-2)$. The inter-cluster mixed valence state is stable at potentials between -0.84 and -1.31 V vs. SSCE, corresponding to ΔE of 470 mV. It has been shown that several factors contribute to ΔE,[13] but the most important contribution here is the stabilization energy imparted to the -1 state by electron delocalization over two Ru_3 cluster cores. The relationship between ΔE and the electronic coupling, H_{AB} has also been discussed.[14–18] A ΔE value of 470 mV corresponds to a comproportionation constant, $K_c = \exp(\Delta EF/RT) = 9.0\times10^7$, for the comproportionation equilibrium relating the -1 state to the neutral and -2 states. The large K_c value here reflects significant thermodynamic stability of the -1 mixed valence state relative to the neutral and -2 states. For the series of complexes $[\{Ru_3(\mu_3\text{-}O)(\mu\text{-}CH_3CO_2)_6(CO)(L)\}_2(\mu\text{-pz})]$, the electron donor/acceptor nature of the terminal ligand (L) has a profound effect on ΔE. This can be understood in terms of the terminal ligand raising or lowering the semi-occupied Ru_3 cluster d-electron levels relative to the pz π^* system. The abco ligand has the highest pK_a (11.15) of the terminal ligands (L) that we have used so far, and the abco complex **1** has the largest ΔE. The abco ligand's ability to increase the electronic interaction between Ru_3 clusters may depend on more than its raising the Ru_3 d-levels into near energetic coincidence with the pz π^* system, however. The pK_a value of a ligand can be related to its ability to direct electron density to a metal center by σ-donation. The electron density at the Ru_3 cores should be reflected by the mean of the reduction potentials ($E_{1/2}(0/-1)$ and $E_{1/2}(-1/-2)$). Figure 4 shows the trend in nitrogen donor ligand pK_a vs. the mean reduction potential ($E_{1/2}$(mean)) for the series of pz bridged Ru_3 dimers. A smooth monotonic trend can be observed between pK_a and $E_{1/2}$(mean), for the three pyridyl ligands (cpy, py, dmap), however the abco ligand stands apart. The abco ligand with the highest pK_a (11.15) has a less negative $E_{1/2}$(mean) than might be expected from the trend, slightly less than the dmap complex. This is further evidence of the fact that the strong donor character of abco as a ligand cannot be fully realized due to steric constraints. Nonetheless, by the ΔE criterion, abco still has the strongest effect on the degree of electronic interaction between the bridged Ru_3 clusters. In contrast to the pyridyl ligands, the abco ligand has no π electron system which can stabilize Ru^{II} by π back donation to some extent. Therefore, two successive one-electron reduction processes in **1** would occur mainly at Ru attached to pz rather than at Ru attached to abco in each Ru_3 unit. This makes the effective distance between the redox centers shorter, and lead to the largest ΔE in spite of the less negative $E_{1/2}$(mean).

Reflectance Infrared Spectroelectrochemistry. The vibrational spectra of complex **1** in its different redox states were obtained by reflectance IR spectroelectrochemistry (SEC).[6,7] However, the doublly reduced inter-cluster mixed valence state ($\mathbf{1}^{2-}$) is too unstable to observe at room temperature. Therefore, a modified variable temperature cell[19] was used, and IR SEC studies were performed at -18 °C. Figure 5 shows IR spectra of the isolated neutral (0), singly (-1), and doubly (-2) reduced states of **1** in the ν(CO) region. The neutral and the doubly reduced compounds show typically sharp single ν(CO) bands at 1937 and 1890 cm^{-1}. The singly reduced species, i.e., the inter-cluster mixed valence compound, shows a broad ν(CO) band centered at 1907 cm^{-1}. Overall, the spectral changes associated with the changes of oxidation state are similar to those for analogous Ru_3 dimers with pyridyl ligands.[6,7] The degree of "coalescence" of the ν(CO) IR band in the inter-cluster mixed valence state depends on the degree of electronic coupling between the pyrazine-linked Ru_3 clusters. On the basis

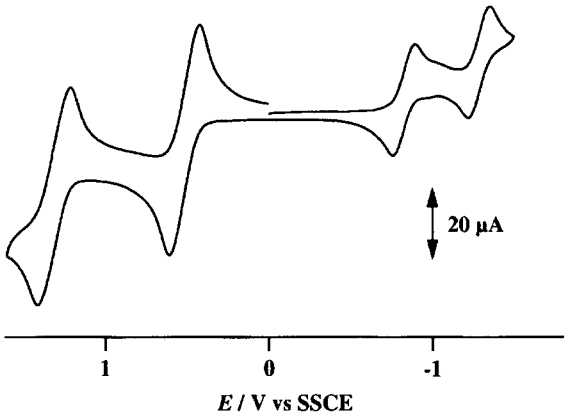

Fig. 3. Cyclic Voltammogram of $[\{Ru_3(O)(CH_3COO)_6(CO)(abco)\}_2(\mu\text{-pz})]$ (**1**) in a 0.1 M $[(n\text{-}C_4H_9)_4N]PF_6$–dichloromethane solution. Scan rate = 100 mV s^{-1}.

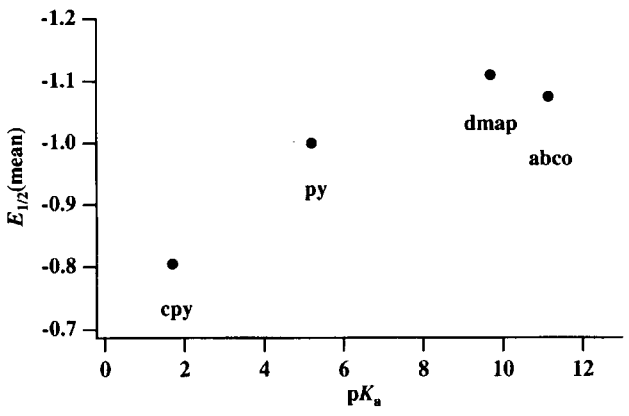

Fig. 4. Relationship between $E_{1/2}$(mean) and pK_a of $[\{Ru_3(O)(CH_3COO)_6(CO)(L)\}_2(\mu\text{-pz})]$, where $E_{1/2}(\text{mean}) = 1/2\{E_{1/2}(0/-1) + E_{1/2}(-1/-2)\}$.

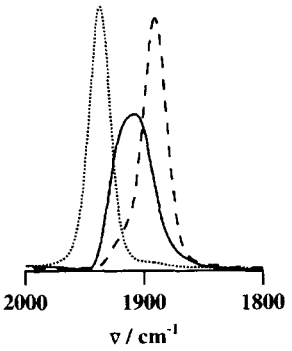

Fig. 5. Infrared spectra for $\mathbf{1}^{n+}$ ($n=0$ (····), -1 (—), -2 (- - -)) in 0.1 M [(n-C_4H_9)$_4$N]PF_6–dichloromethane solution, -18°C.

of ΔE, derived from electrochemical data, and H_{AB}, derived from the intervalence charge transfer (ICT) band (vide infra), $\mathbf{1}^-$ is the most strongly coupled of the series of [{$Ru_3(\mu_3$-O)(μ-$CH_3CO_2)_6$(CO)(L)}$_2$(μ-pz)] complexes yet prepared. Prior to the present study, the L = dmap cluster had the most strongly coupled mixed valence state. The values of ΔE and H_{AB} for the abco vs. dmap substituted mixed valence complexes are 470 vs. 440 mV and 2490 vs. 2180 cm^{-1}, respectively. These data predict the observed result: the ν(CO) lineshape of $\mathbf{1}^-$ is the narrowest and most fully coalesced that we have observed. We estimate a rate constant for intramolecular electron transfer in $\mathbf{1}^-$ from the NMR-like Bloch equation analysis described previously.[6,7,20] Figure 6 shows the simulated IR spectral lineshapes as a function of k_e and a comparison to the observed spectrum of $\mathbf{1}^-$. The electron transfer rate constant estimated by this type of simulation for $\mathbf{1}^-$ is $(1.0\pm0.3)\times10^{12}$ s^{-1} at -18 °C, which is slightly but not significantly faster than that for dmap analogue $(0.9\pm0.3)\times10^{12}$ s^{-1} at room temperature.

We attempted also to study the temperature dependence of IR spectrum of $\mathbf{1}^-$ with the variable temperature cell.[19] The ν(CO) band shape did not change within experimental error over the temperature range -40 °C to room temperature. The essentially temperature independent rate constant is perhaps not surprising. The electron transfer rate constant obtained here, $(1.0\pm0.3)\times10^{12}$ s^{-1}, is nearly the solvent collisional rate constant (ca. 10^{12} s^{-1}),[21] which is the pre-exponential term in the rate equation. This indicates that $\Delta G^{\ddagger}$ is very small, possibly < 1 kcal mol^{-1}. Under such situations, the rate constant would be temperature independent.

Intervalence Charge Transfer. In order to assess further the extent of electronic interaction between the two coupled Ru_3 units in the -1 states, intervalence charge transfer (ICT) spectra were examined. Figure 7 shows the electronic absorption spectra of the neutral, -1, and -2 states of **1**. The neutral species exhibits no absorptions in the near IR region. Upon reduction to the -1 state, new, broad bands appear. The spectrum of $\mathbf{1}^-$ shows strong low energy absorption bands at $\tilde{\nu}_{max}=12500$ cm^{-1} ($\varepsilon=15300$ M^{-1} cm^{-1}) and $\tilde{\nu}_{max}=7200$ cm^{-1} ($\varepsilon=10350$ M^{-1} cm^{-1}) (1 M = 1 mol dm^{-3}). Since cluster to cluster intervalence charge transfer (ICT) should appear only in the -1 state ($Ru^{III}_2Ru^{II}$–pz–$Ru^{III}Ru^{II}_2$), the

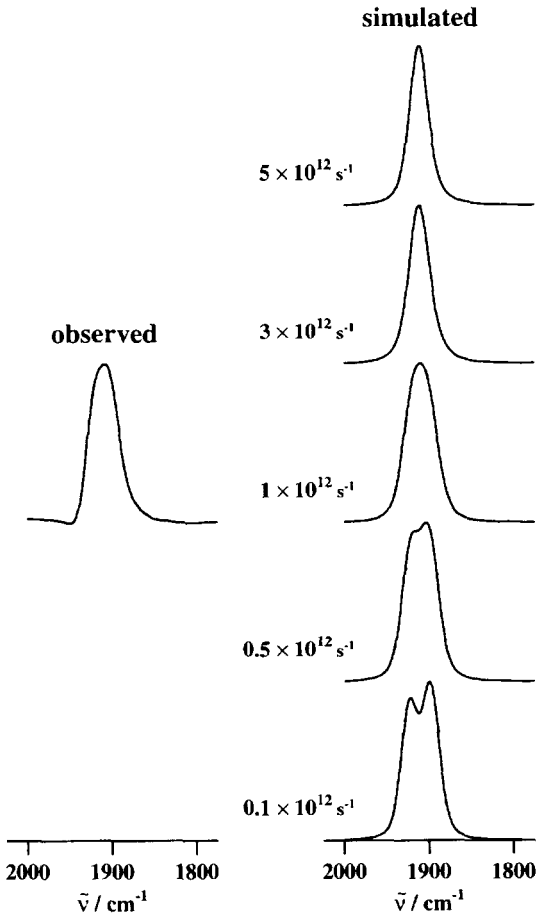

Fig. 6. Comparison of observed to simulated infrared spectra for the mixed valence state of $\mathbf{1}^-$ as a function of the intramolecular electron transfer rate constant, k_e.

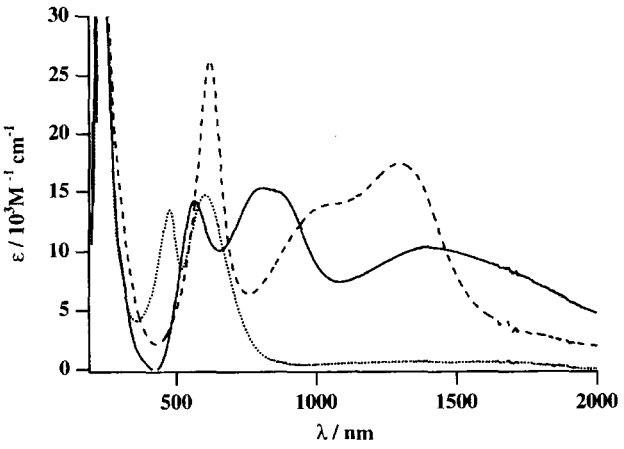

Fig. 7. Electronic absorption spectral data for **1** in the neutral isolated ($n=0$, (····)), 1-electron reduced ($n=-1$, (—)), and 2-electron reduced ($n=-2$, (- - -)) states, 0.1 M [(n-C_4H_9)$_4$N]PF_6–dichloromethane solution, -35°C.

band at $\tilde{\nu}_{max}=12500$ cm^{-1} is assigned to be the ICT absorption of $\mathbf{1}^-$. The band at $\tilde{\nu}_{max}=7200$ cm^{-1} may be assigned to intra-cluster transition(s) within the $Ru^{III}Ru^{II}_2$ unit. The -2 state of **1** also exhibits a band at nearly the same energy with double intensity, in support of this assignment. We note also

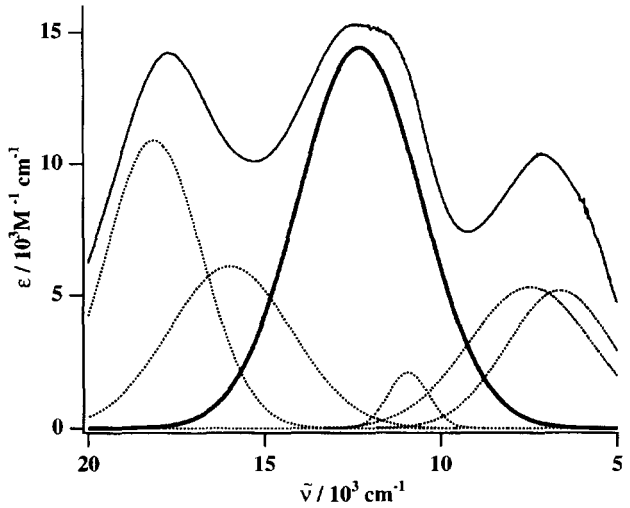

Fig. 8. Electronic absorption spectral data for **1** in the 1-electron reduced ($n=-1$) states in 0.1 M $[(n\text{-}C_4H_9)_4N]PF_6$– dichloromethane solution, −35°C (solid line), and the deconvoluted ICT band (dotted line). Solid bold line corresponds to the single Gaussian fit of the ICT band.

that the related monomeric compound, $[Ru_3^{III,II,II}(\mu_3\text{-}O)(\mu\text{-}CH_3CO_2)_6(CO)(dmap)_2]^-$, shows a band with a shoulder on the high energy side, very similar to that observed at 7700 cm^{-1} for $\mathbf{1}^{2-}$. These facts support the assignments of ICT absorption at $\tilde{\nu}_{max}=12500$ cm^{-1} and intra-cluster absorption at 7200 cm^{-1}.

Inter-cluster electronic coupling, H_{AB}, was estimated by deconvolution of the ICT spectra of **1** (Fig. 8).

Reasonably good agreement between the observed spectra of $\mathbf{1}^-$ and the sum of deconvoluted spectral components was obtained. It was assumed that the ICT band consists of a single Gaussian band shape and that the intracluster transitions at longer wavelength have three components. The spectral data of the deconvoluted ICT band are $\tilde{\nu}_{max}=12300$ cm^{-1}, $\varepsilon = 14400$ M^{-1} cm^{-1}, $\Delta\tilde{\nu}_{1/2}=4100$ cm^{-1}. The electronic coupling H_{AB}, derived from the optical spectra of the singly reduced (−1) charge transfer states, is given by Eq. 3.[3]

$$H_{AB} = 2.05 \times 10^{-2} (\tilde{\nu}_{max} \varepsilon_{max} \Delta\tilde{\nu}_{1/2})^{1/2}/r. \quad (3)$$

The optical estimate of H_{AB},[22] is 2490 cm^{-1}, which is the largest determined for an inter-cluster mixed valence state of a pz-bridged ruthenium cluster complex of the type $[\{Ru_3(\mu_3\text{-}O)(\mu\text{-}CH_3CO_2)_6(CO)(L)\}_2(\mu\text{-pz})]$.

Experimental

Materials. $[Ru_3(O)(CH_3CO_2)_6(CO)(C_2H_5OH)_2]$[23] was synthesized according to the reported method. Tetra-*n*-butylammonium hexafluorophosphate $[(n\text{-}C_4H_9)_4N]PF_6$ was prepared according to the reported method.[10] Other reagents were used as received.

Preparations. **$[Ru_3(O)(CH_3CO_2)_6(CO)(abco)_2]$ (2).** A mixture of $[Ru_3(O)(CH_3CO_2)_6(CO)(C_2H_5OH)_2]$ (250 mg, 0.315 mmol) and abco (375 mg, 3.37 mmol) in CH_3OH (30 cm^3) was allowed to stand for 2 d at room temperature. The solution was evaporated to dryness using a rotary evaporator, and the residue was dissolved in a minimal amount of $CHCl_3$. The solution was placed on a column packed with silica gel (Wakogel C-200), and a mixture of $CHCl_3/C_2H_5OH$ (99.0/1.0, v/v) was used as the eluent. The main fraction was collected and evaporated to dryness. The residue was dissolved in a small amount of CH_2Cl_2, and excess *n*-hexane was added to the solution. A blue precipitation was collected by filtration. (yield: 175 mg, 60%). Anal. Calcd for **2**·$CHCl_3$: C, 32.24; H, 4.35; N, 2.69%. Found: C, 32.59; H, 3.94; N, 2.70%. ^1H NMR in $CDCl_3$ $\delta = 1.68$ (6H, acetate methyl), 2.00 (12H, acetate methyl), 2.27 (12H, abco methylene), 2.40 (2H, abco methyne), 3.77 (12H, abco methylene). IR (KBr pellet) ν(CO) = 1941 cm^{-1}. MS (FAB) *m/z* 897 ([**2**–CO]). UV-vis λ_{max} (ε/dm^3 mol^{-1} cm^{-1}) in CH_2Cl_2 300 (5000), 384 (2000), 570 (3000) nm. CV data in CH_2Cl_2: $E_{1/2}$ = +1.31 (+2/+1), 0.43 (+1/0), E_{pc} = −1.50 (0/−1) V vs. SSCE.

$[\{Ru_3(O)(CH_3CO_2)_6(CO)(abco)\}_2(\mu\text{-pz})]$ (1). A mixture of **2** (250 mg 0.270 mmol) and pz (11mg 0.137 mmol) in CH_2Cl_2 (30 cm^3) was refluxed for 1 d, during which time the color changed from blue to blue-green. The solution was evaporated to dryness using a rotary evaporator, and the residue was dissolved in a minimal amount of $CHCl_3$ and filtered. The filtrate was subjected to column chromatography (Bio beads S-X3). The main fraction was collected and evaporated to dryness, and the residue was dissolved in a minimal amount of $CHCl_3$. The solution was placed on a chromatographic column packed with silica gel (Wakogel C-200), and a mixture of $CHCl_3/C_2H_5OH$ (98.5/1.5, v/v) was used as the eluent. The main fraction was collected and evaporated to dryness. The residue was dissolved in a small amount of CH_2Cl_2, and excess *n*-hexane was added to the solution. A deep-blue precipitation was collected by filtration. Yield: 68 mg (30%). Anal. Calcd for **1**·$CHCl_3$: C, 29.62; H, 3.70; N, 3.07%. Found: C, 29.99; H, 3.62; N, 3.03%. ^1H NMR in $CDCl_3$ $\delta = 1.92$ (12H, acetate methyl), 2.09 (12H, acetate methyl), 2.18 (12H, acetate methyl), 2.29 (12H, abco methylene), 2.43 (2H, abco methyne), 3.76 (12H, abco methylene), 9.28 (4H, pz). IR (KBr pellet) ν(CO) = 1948 cm^{-1}. FAB MS *m/z* 1649 ([**1**–2CO]). UV-vis λ_{max} (ε/dm^3 mol^{-1} cm^{-1}) in CH_2Cl_2 481 (14500), 598 (14700) nm.

Measurements. Electronic absorption spectra were recorded on a Shimadzu UV-3100PC spectrometer. ^1H NMR spectra were obtained on a JEOL GSX-270 FT NMR spectrometer at 270 MHz. Chemical shifts are reported with respect to an internal reference of TMS in $CDCl_3$.

Cyclic voltammetry (CV) and differential-pulse voltammetry (DPV) were performed using a BAS CV-50W voltammetric analyzer. A glassy carbon electrode was used as the working electrode. The counter electrode was a platinum coil, and the reference electrode was a saturated sodium calomel electrode (SSCE). CV was performed at a scan rate of 100 mV s^{-1}. All the half-wave potentials $E_{1/2} = (E_{pc}+E_{pa})/2$, where E_{pc} and E_{pa} are the cathodic and anodic peak potential, respectively, are reported with respect to the SSCE in this study.

Controlled-potential absorption spectra were obtained with an optically transparent thin-layer electrode (OTTLE) cell. The optical path length was 0.5 mm. The working electrode was platinum mesh. The counter electrode was a platinum coil. The reference electrode was an SSCE. The OTTLE cell was cooled to ca. −35 °C. Spectroelectrochemical experiments were carried out in 0.1 M tetra-*n*-butylammonium hexafluorophosphate solutions using spectrochemical grade dichloromethane. All solutions were prepared under an atmosphere of nitrogen and deoxygenated completely by N_2 gas before injection into the OTTLE cell. A Hokutodenko HA-501 potentiostat was used to effect and monitor thin layer bulk electrolyses. The vis-NIR spectra were recorded on a Shimadzu UV-3100PC spectrometer.

IR spectral changes accompanying thin-layer bulk electrolyses were measured using the modified[19] temperature controlled flow-through reflectance spectroelectrochemical (SEC) cell reported earlier.[24] Pathlengths were typically 0.2 mm. The controlled potentials were measured vs. Ag pseudo-reference electrode (ca. −0.06 V vs. SCE). Spectroelectrochemical experiments were carried out in 0.1 M tetra-*n*-butylammonium hexafluorophosphate solutions using spectrochemical grade dichloromethane. All solutions were prepared under an atmosphere of nitrogen and deoxygenated completely by N_2 gas before injection into the SEC cell. Blank reference solutions containing 0.1 M tetra-*n*-butylammonium hexafluorophosphate were used for the Fourier Transform IR solvent subtractions. Spectral baseline shifts in the different redox states were adjusted. Normal measurements were performed at −18 °C and temperature dependence studies were performed from room temperature to −40 °C. A Hokutodenko HA-501 potentiostat was used to effect and monitor thin layer bulk electrolyses. The IR spectra were acquired using a JASCO FT/IR-620 spectrophotometer.

All electrochemical and spectroelectrochemical measurements were carried out under a nitrogen atmosphere.

X-Ray Structural Analysis of 1·2CH_2Cl_2. Single crystals of **1**·2CH_2Cl_2 suitable for X-ray crystallography were obtained by slow recrystallization of **1** in a mixed CH_2Cl_2/hexane solution at room temperature. A deep violet prismatic crystal of **1**·2CH_2Cl_2 was attached to the top of a glass fiber and coated with an epoxy resin, and it was then mounted on a BRUKER AXS SMART 1000 diffractometer with graphite-monochromated Mo $K\alpha$ (λ = 0.71073 Å) radiation. The X-ray data were collected at −70 °C. Lorentz, polarization, and absorption correction (SADABS[25]) were applied to the intensity data. The structure was solved by Patterson analysis method using the DIRDIF92 PATTY program.[26] The abco ligand is disordered at two positions holding in common nitrogen and methyne carbon, and two sets of ethylene chains with 0.75 and 0.25 occupancy were used for refinement. A disorder was also observed for chlorine atoms of solvate dichloromethane, and two sets of two chlorine atoms with 0.5 occupancy were located. All non-hydrogen atoms and hydrogen atoms of acetate and pyrazine were located by Fourier synthesis and full-matrix least-squares. Non-hydrogen atoms except for disordered atoms were refined anisotropically. All calculations were performed with use of the teXsan[27] crystallographic software package incorporated with SHELXL-93.[28]

X-Ray Structural Analysis of 2·CH_2Cl_2. Single crystals of **2**·CH_2Cl_2 suitable for X-ray crystallography were obtained by slow recrystallization of **2** in a mixed CH_2Cl_2/hexane solution at room temperature. A deep violet prismatic crystal of **2**·CH_2Cl_2 was attached to the top of a glass fiber and coated with an epoxy resin, and it was then mounted on a BRUKER AXS SMART 1000 diffractometer with graphite-monochromated Mo $K\alpha$ (λ = 0.71073 Å) radiation. The X-ray data were collected at room temperature. Lorentz, polarization, and absorption correction (numerical integration) were applied to the intensity data. The structure was solved by Patterson method. The abco ligand is disordered at two positions holding in common nitrogen and methyne carbon, and two sets of ethylene chains with 0.5 occupancy were used for refinement. All non-hydrogen atoms were located by Fourier synthesis and full-matrix least-squares and were refined anisotropically.

Crystallographic data have been deposited at the CCDC, 12 Union Road, Cambridge CB2 1EZ, UK and copies can be obtained on request, free of charge, by quoting the publication and the deposition numbers CCDC 141261-141262. The data are also deposited as Document No. 73031 at the Office of the Editor of Bull. Chem. Soc. Jpn.

This work was supported by Grant-in-Aids for Scientific Research Priority Area No. 10149102 "Metal Assembled Complexes" and International Scientific Research Program (No. 11694051) from the Ministry of Education, Science, Sports and Culture. CPK gratefully acknowledges support from the National Science Foundation (CHE-9615886).

References

1 M. B. Robin and P. Day, *Adv. Inorg. Chem. Radiochem.*, **10**, 247 (1967).

2 C. T. Dziobkowski, J. T. Wrobleski, and D. B. Brown, *Inorg. Chem.*, **20**, 679 (1981).

3 N. S. Hush, *Prog. Inorg. Chem.*, **8**, 391 (1967).

4 R. Wu, S. K. Arap Koske, R. P. White, C. E. Anson, U. A. Jayasooriya, and R. D. Cannon, *J. Chem. Soc., Chem. Commun.*, **1994**, 1657.

5 A. Masuda, Y. Masuda, and Y. Fukuda, *J. Phys. Chem. A*, **101**, 2245 (1997).

6 T. Ito, T. Hamaguchi, H. Nagino, T. Yamaguchi, J. Washington, and C. P. Kubiak, *Science*, **277**, 660 (1997).

7 T. Ito, T. Hamaguchi, H. Nagino, T. Yamaguchi, H. Kido, I. S. Zavarine, T. Richmond, J. Washington, and C. P. Kubiak, *J. Am. Chem. Soc.*, **121**, 4625 (1999).

8 H. Kido, H. Nagino, and T. Ito, *Chem. Lett.*, **1996**, 745.

9 S. Campagna, G. Denti, S. Serroni, M. Ciano, A. Juris, and V. Balzani, *Inorg. Chem.*, **31**, 2982 (1992).

10 M. Abe, Y. Sasaki, Y. Yamada, K. Tsukahara, S. Yano, T. Yamaguchi, M. Tominaga, I. Taniguchi, and T. Ito, *Inorg. Chem.*, **35**, 6724 (1996).

11 M. Abe, Y. Sasaki, T. Yamaguchi, and T. Ito, *Bull. Chem. Soc. Jpn*, **65**, 1585 (1992).

12 K. Ota, H. Sasaki, T. Matsui, T. Hamaguchi, T. Yamaguchi, T. Ito, H. Kido, and C. P. Kubiak, *Inorg. Chem.*, **38**, 4070 (1999).

13 F. Salaymeh, S. Berhane, R. Yusof, R. de la Rosa, E. Y. Fung, R. Matamoros, K. W. Law, Q. Zheng, E. M. Kober, and J. C. Curtis, *Inorg. Chem.*, **32**, 3895 (1993).

14 D. E. Richardson and H. Taube, *Coord. Chem. Rev.*, **60**, 107 (1984).

15 D. E. Richardson and H. Taube, *Inorg. Chem.*, **20**, 1278 (1981).

16 J. E. Sutton and H. Taube, *Inorg. Chem.*, **20**, 3125 (1981).

17 R. de la Rosa, P. J. Chang, F. Salaymeh, and J. C. Curtis, *Inorg. Chem.*, **24**, 4229 (1985).

18 Y. Dong and J. T. Hupp, *Inorg. Chem.*, **31**, 3170 (1992).

19 I. S. Zavarine, T. A. Richmond, and C. P. Kubiak, *J. Electroanal. Chem.*, submitted.

20 F.-W. Grevels, K. Kerpen, W. E. Klotzbucher, R. E. D. McClung, G. Russel, M. Viotte, and K. Schaffner, *J. Am. Chem. Soc.*, **120**, 10423 (1998).

21 a) D. Astruc,"Electron Transfer and Radical Processes in Transition-Metal Chemistry," VCH Publishers, Weinheim (1995). b) J. W. Moore and R. G. Pearson, "Kinetics and Mechanism, A Study of Homogeneous Chemical Reactions," 3rd ed, John Wiley & Sons, New York (1981).

22 The distance r was use of the shortest Ru–Ru distance bridged by pyrazine (Ru1–Ru1′ = 7.011 Å).

23 J. A. Baumann, S. T. Wilson, D. J. Salmon, P. L. Hood, and T. J. Meyer, *J. Am. Chem. Soc.*, **101**, 2916 (1979).

24 R. E. Wittrig and C. P. Kubiak, *J. Electroanal. Chem.*, **393**,

75 (1995).

25 G. M. Sheldrick, "SADABS, a program for absorption correction of areadetector data," University of Göttingen, Germany (1996).

26 P. T. Beurskens, G. Admiraal, G. Beurskens, W. P. Bosman, S. Garcia-Granda, R. O. Gould, J. M. M. Smits, and C. Smykalla, "The DIRDIF program system, Technical Report of the Crystallography Laboratory," University of Nijmegen, The Netherlands (1992).

27 "teXsan, single crystal structure analysis software, version 1.7," Molecular Structure Corporation, The Woodlands, TX (1995).

28 G.M. Sheldrick, "SHELXL-93, a program for the refinement of crystal structuers," University of Göttingen, Germany (1993).